Journal of Power Sources 229 (2013) 203–209

Contents lists available at SciVerse ScienceDirect

Journal of Power Sources

journal homepage: www.elsevier.com/locate/jpowsour

Synthesis of nano-sized $LiMnPO_4$ and in situ carbon coating using a solvothermal method

Jiali Liu, Xiaoyu Liu, Tao Huang, Aishui Yu*

Department of Chemistry and Shanghai Key Laboratory of Molecular Catalysis and Innovative Materials, Institute of New Energy, Fudan University, 2205 Songhu Road, Shanghai 200433, China

HIGHLIGHTS

- Nano-sized $LiMnPO_4$ was synthesized via mild solvothermal method.
- A favorable configuration with $LiMnPO_4$ particles embedded in carbon was formed.
- The composite displayed a specific capacity of over 130 mAh g^{-1} at 0.1 C.
- The lithium diffusion constants were estimated by EIS measurements.

ARTICLE INFO

Article history:
Received 15 August 2012
Received in revised form
7 October 2012
Accepted 24 November 2012
Available online 12 December 2012

Keywords:
Nano-sized
In situ carbon coating
Lithium manganese phosphate
Lithium ion battery
Discharge capacity

ABSTRACT

Nano-sized lithium manganese phosphate ($LiMnPO_4$) is successfully prepared using a mild solvothermal method in ethylene glycol solvent. The particle size, observed by Scanning Electron Microscopy (SEM), is approximately 100 nm using C_6H_5COOLi as the starting material. Further TEM characterization reveals that the decomposition of benzoyloxy in this lithium salt leads to a favorable configuration, with $LiMnPO_4$ particles embedded in carbon and a distinct in situ carbon layer formed even on partial particles. Using subsequent heat-treatment with a certain amount of sucrose, $LiMnPO_4$/C composites that display a good two-phase plateau during the discharge process can be formed, with a specific capacity over 130 mAh g^{-1} at 0.1 C.

1. Introduction

Olivine-structured lithium transition-metal phosphate has attracted broad attention as a potential Li-ion battery cathode material to replace transition metal oxide-based materials such as $LiCoO_2$ [1,2]. This family of phosphate compounds has a three-dimensional framework stabilized by strong covalent bonds between oxygen ions and P^{5+}, resulting in PO_4^{3-} tetrahedral poly-anions [3–5]. These lithium transition-metal phosphate materials show better reversible capacity and higher stability without structural rearrangement during lithiation and de-lithiation [5–7]. $LiMPO_4$ is therefore the best choice for use in a number of applications including Electric Vehicle and Hybrid-Electric Vehicle [8–10].

Lithium manganese phosphate ($LiMnPO_4$) has a higher redox voltage plateau of 4.1 V for Mn^{2+}/Mn^{3+} versus Li^+/Li, indicating its higher energy density [11,12]. However, its intrinsic low electronic and ionic conductivity limits its electrochemical behavior [13,14]. Some research groups have suggested that the extraction of Li^+ from $LiMnPO_4$ is negligible [15–17]. To improve the performance of $LiMnPO_4$, several methods have focused on decreasing the particle size and carbon coating. Among these, hydrothermal/solvothermal methods have been employed to control the morphology and texture of the material. G. S. Li revealed that one-dimensional rods of $LiMnPO_4$ could be obtained through inhibition of CO_3^{2-} via hydrothermal/solvothermal process [18]. Y. T. Qian prepared nanosquare $LiMnPO_4$ with an edge size of 800–1000 nm and a thickness of 50–250 nm using a hydrothermal process with $Na_4P_2O_7 \cdot 10H_2O$ as starting material. The initial discharge capacity was 125.5 mAh g^{-1} at 0.1 C and maintained 86.7% of its initial capacity after 50 cycles [19]. D. Rangappa reported the preparation of nanocrystalline $LiMnPO_4$ under supercritical fluid conditions

* Corresponding author. Tel./fax: +86 21 51630320.
E-mail address: asyu@fudan.edu.cn (A. Yu).

0378-7753/$ – see front matter © 2012 Elsevier B.V. All rights reserved.
http://dx.doi.org/10.1016/j.jpowsour.2012.11.093

[20]. Here, nano-sized $LiMnPO_4$ is successfully prepared with some new organic lithium salt as starting material and EG as the medium using a mild solvothermal process. The typical particle size is approximately 100–200 nm, and these particles are dispersed well. Moreover, there's no doubt that in situ carbon coating in solution is the most effective way to improve the electronic conductivity for its well distributed. H. S. Zhou et al. employed in situ polymerization method in the precipitation process to prepare $LiFePO_4$/C nanocomposite with core–shell structure and it showed excellent electrochemical behavior [21]. Some groups have prepared $LiMPO_4$ (M = Mn, Fe, Co) particles coated with an in situ carbon layer generated from decomposition of high concentrations of glucose in the hydrothermal precursor solution [22,23]. And the electrochemical behavior of in situ carbon coating samples was better than that of mixed coating. Here in our work, in situ coating carbon could also be obtained by decomposition of the organic group in the lithium salt during the solvothermal treatment. With subsequent heat-treatment with sucrose, the $LiMnPO_4$/C composite displayed a discharge capacity of 130 mAh g^{-1} at 0.1 C. Hence, we suggest that further research may lead to an excellent cathode candidate for lithium ion batteries.

2. Experimental

2.1. Synthesis of materials

We used common organic lithium salts as the starting material, and all chemicals were used without pretreatment or purification. C_6H_5COOLi (Lithium benzoate), CH_3COOLi (lithium acetate), and $C_5H_7LiO_2$ (2,4-pentanedionato lithium) were used as lithium salts. $MnSO_4 \cdot 2H_2O$, $NH_4H_2PO_4$, and citric acid were all dissolved in EG (ethylene glycol) with stirring to give Li:Mn:P equal to 3:1:1. $NH_3 \cdot H_2O$ was used to adjust the pH to 10, and the mixture was transferred to a 50-ml Teflon-lined reactor tightly sealed inside a stainless steel reactor. After treatment at 250 °C or 270 °C for 12–15 h, the precipitate was filtered and washed several times with deionized water and ethanol. To improve conductivity and crystallization, $LiMnPO_4$ was mixed with sucrose and annealed at 550 °C for 3 h in an Ar atmosphere containing 5% H_2.

2.2. Characterization

X-ray diffraction (XRD) measurements were carried out on a Bruker D8 Advance X-ray diffractometer using a Cu K_α radiation source (λ = 1.5406 Å) with a step size of 4° min^{-1} from 10 to 80°. The powder morphology was observed using a scanning electron microscope (SEM, JEOL JSM-6390) and transmission electron microscope (TEM, CM200FEG). Inductively coupled plasma (ICP, Thermo E.IRISDuo) and atomic absorption spectroscopy (AAS, Z-5000) were used to analyze the Li, Fe, and P content of all the samples. The carbon content in the $LiMnPO_4$/C composite was measured using a carbon–sulfur analyzer (Eltra CS800).

2.3. Electrochemical measurements

The electrochemical performance of the prepared $LiMnPO_4$ was investigated using coin cells assembled in an argon-filled glove box (SIMATIC OP7, MBRAUN). The cell was composed of a lithium anode and a cathode that was a mixture of prepared $LiMnPO_4$ (70%), Super P Carbon black (20%) and polytetrafluroethylene (PTFE) (Dupont) (10%). The mixture was rolled into a thin sheet with uniform thickness and cut into 10 mm × 10 mm sections before being pressed into an aluminum mesh. Typical loading of the active material was approximately 10 mg cm^{-2}. The electrolyte was 1 M $LiPF_6$ dissolved in a mixture of ethylene carbonate (EC) and dimethyl carbonate (DMC) (1:1 w/w), and Celgard 2300 was used as separator. Electrochemical (EIS) measurements were performed on a CHI660 B electrochemical analysis instrument. The charge–discharge and cycling properties were evaluated on Land CT 2001A electrochemical measurements system between 2.5 and 4.5 V at various rate (1 C = 140 mAh g^{-1}). All tests were performed at room temperature.

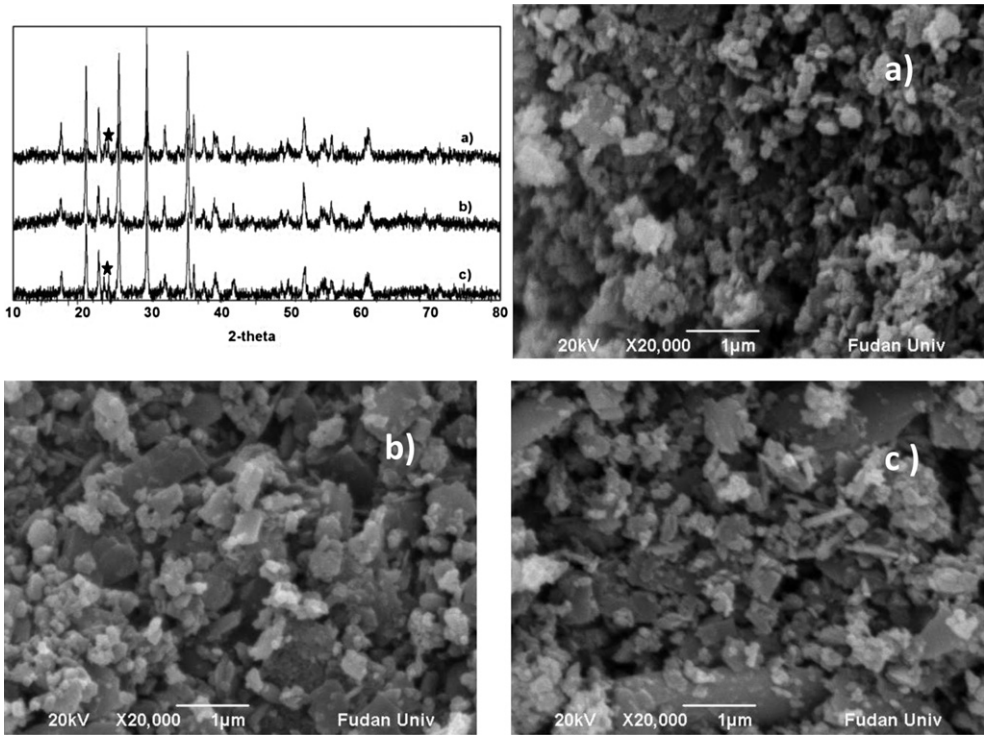

Fig. 1. XRD and SEM data of samples with different lithium salts at 250 °C for 12 h: a) C_6H_5COOLi, b) CH_3COOLi, c) $C_5H_7LiO_2$. Labeled peaks indicate the impurity phase.

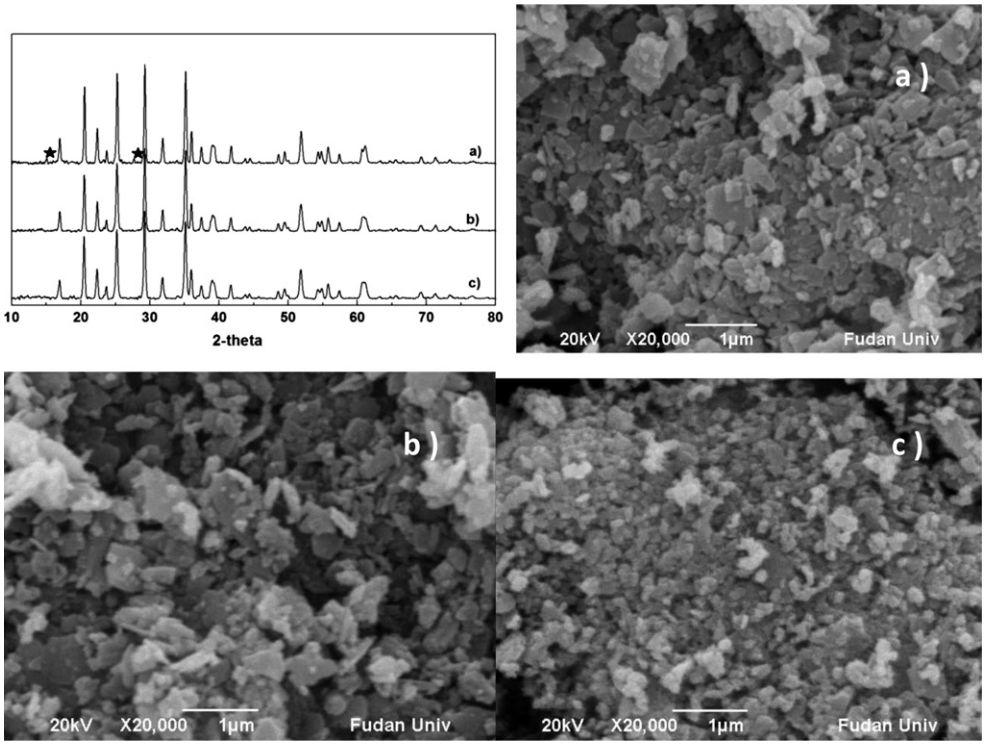

Fig. 2. XRD and SEM data of samples with different lithium salts at 270 °C for 12 h: a) C_6H_5COOLi, b) CH_3COOLi, c) $C_5H_7LiO_2$. Labeled peaks indicate the impurity phase.

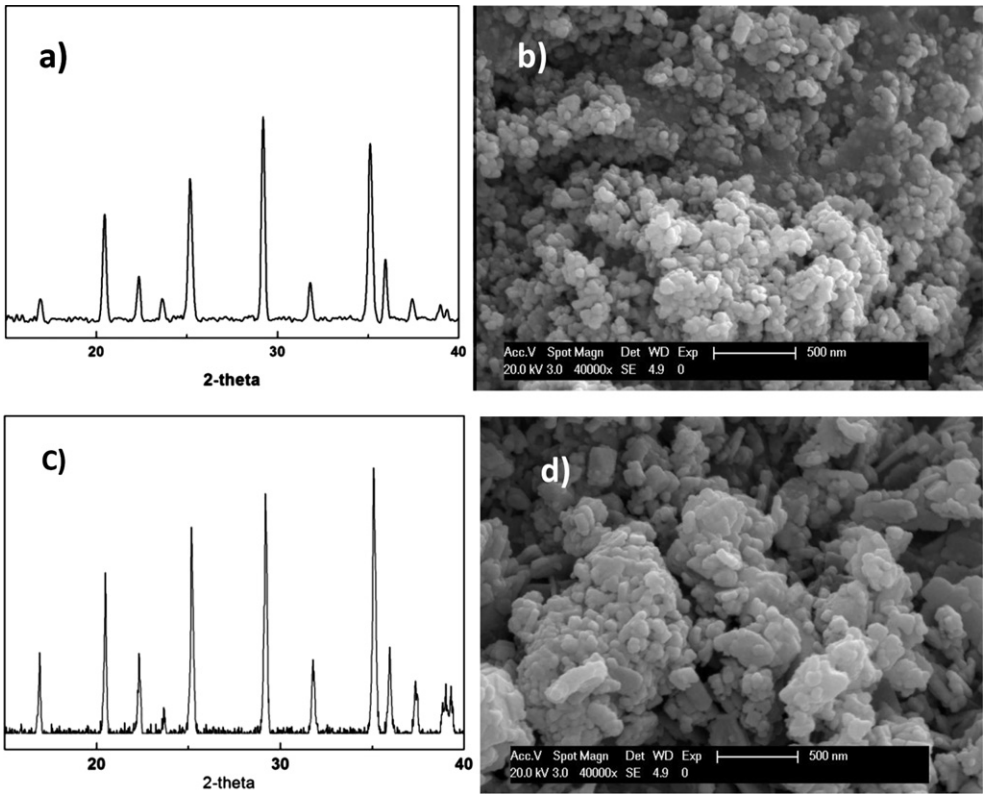

Fig. 3. XRD and SEM data of $LiMnPO_4$ samples: a), b) 250 °C 15 h for C_6H_5COOLi, c), d) 270 °C 15 h for $C_5H_7LiO_2$.

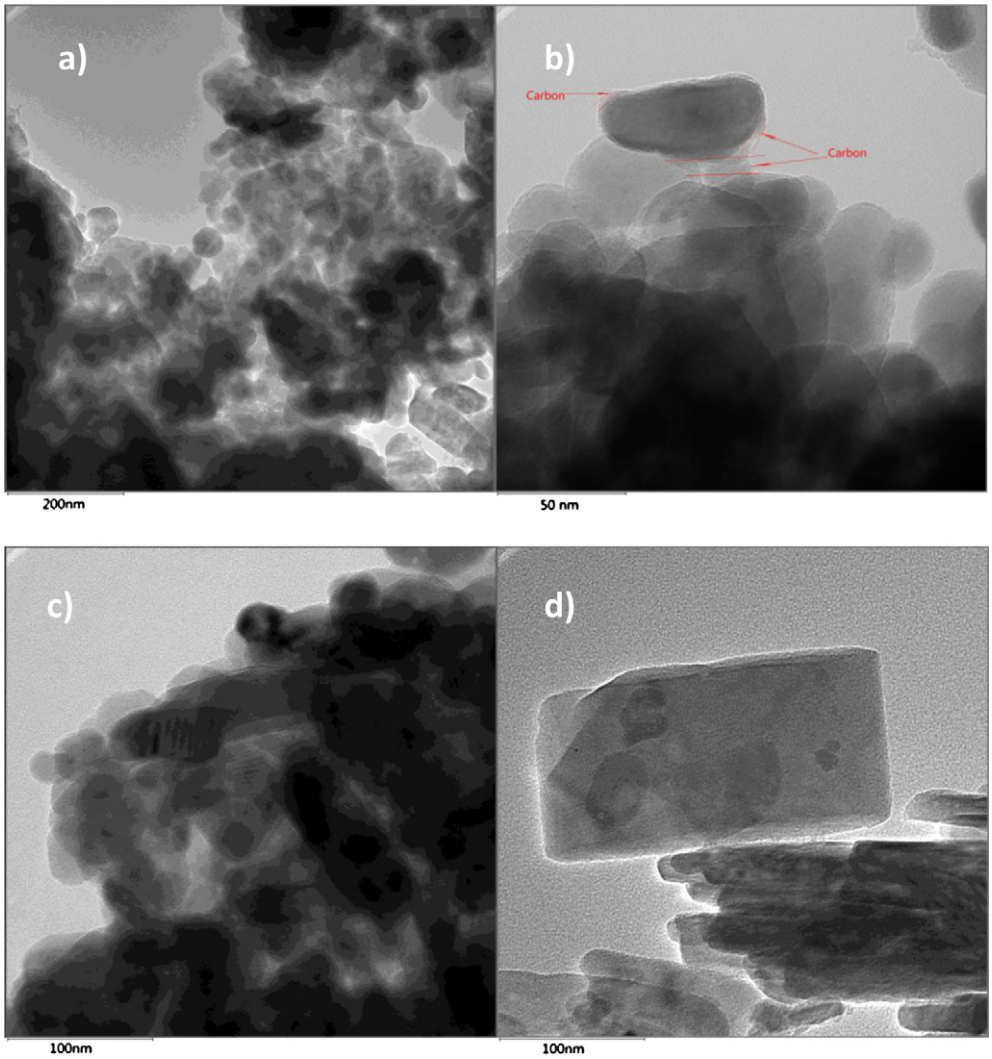

Fig. 4. TEM photos of $LiMnPO_4$ samples: a), b) 250 °C 15 h for C_6H_5COOLi, c) 250 °C 15 h for CH_3COOLi, d) 270 °C 15 h for $C_5H_7LiO_2$.

3. Results and discussion

3.1. Material identification

Fig. 1 shows XRD data of the samples obtained with organic lithium salts at 250 °C for 12 h. As expected, highly crystalline $LiMnPO_4$ product was formed, but some impurities were found with C_6H_5COOLi and $C_5H_7LiO_2$. The labeled peaks indicate these impurity phases. SEM measurements were carried out on the $LiMnPO_4$ samples, and the photos are displayed in Fig. 1. Powders obtained with CH_3COOLi (Fig. 1b) show sheet-like, randomly oriented particles with length less than 1 μm, consistent with previous studies [18,22]. There were some morphological changes with the change of lithium salt. 100 nm-sized particles in diameter that were very well-dispersed could be observed for C_6H_5COOLi (Fig. 1a). Randomly aggregated sheet-like particles were also obtained with $C_5H_7LiO_2$ (Fig. 1c). Hence, lithium salt had a significant effect on the morphology of $LiMnPO_4$ obtained solvothermally.

To illustrate the effect of reaction temperature, the solvothermal process was held at a constant 270 °C for 12 h. Fig. 2 shows the XRD data, which is similar to that of Fig. 1. All samples showed well-ordered, olivine-structured $LiMnPO_4$, and impurities were also observed for C_6H_5COOLi and $C_5H_7LiO_2$. Some morphological differences compared to samples obtained at 250 °C are visible in the SEM photos shown in Fig. 2. Samples generated with C_6H_5COOLi and CH_3COOLi were sheet-like particles less than 1 μm (Fig. 2a,b). Conversely, well-dispersed 100-nm-sized particles were obtained for $C_5H_7LiO_2$ under this condition (Fig. 2c).

According to previous studies, the phase composition of $LiMnPO_4$ obtained using hydrothermal methods was related to the reaction time and temperature [23]. Hence, to obtain $LiMnPO_4$ without any impurities, we increased the reaction duration to 15 h at 250 °C for C_6H_5COOLi and 270 °C for $C_5H_7LiO_2$. The XRD and SEM

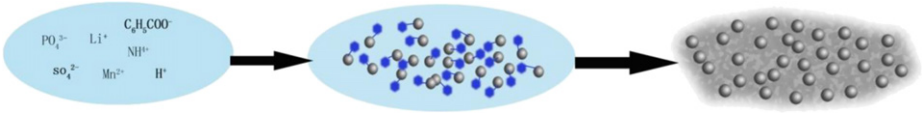

Scheme 1. Formation mechanism for $LiMnPO_4$ with C_6H_5COOLi.

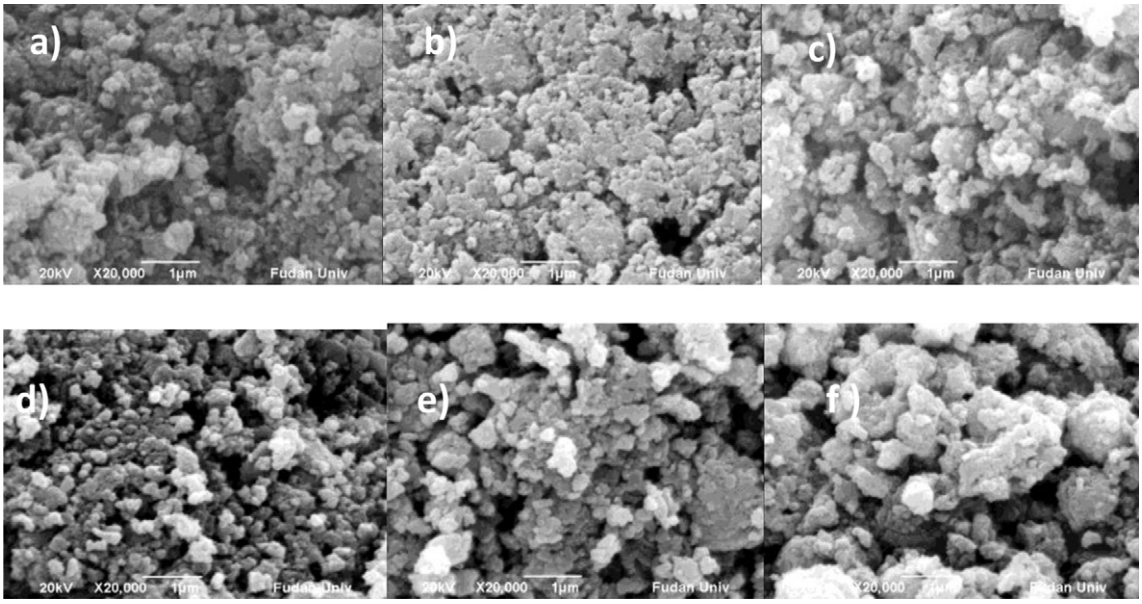

Fig. 5. SEM data of $LiMnPO_4$/C samples with varying sucrose concentration: a) 20%, b) 30%, c) 40% and C_6H_5COOLi, d) 20%, e) 30%, f) 40% for $C_5H_7LiO_2$.

data are displayed in Fig. 3: well-crystallized $LiMnPO_4$ without any impurities were obtained under this condition (Fig. 3a,c). No obvious adverse morphological effects were found for C_6H_5COOLi, and the particles were still approximately 100 nm (Fig. 3b). However, slight agglomeration and partial plate-like particles were visible for $C_5H_7LiO_2$ (Fig. 3d).

To further analyze the amount of Li, Fe, P in the $LiMnPO_4$ samples with C_6H_5COOLi and $C_5H_7LiO_2$ as precursors, ICP-AAS measurement was employed. The Li amount was determined by AAS analysis, and Fe and P by ICP to reveal the stoichiometric atom ratio for these two samples. Previous literature has suggested that reaction temperature and time play a critical role in the morphology and purity of $LiMnPO_4$ samples obtained via hydrothermal methods. Our experiments strongly confirm this hypothesis. In addition, we suggest that lithium salts are also a vital factor. It has been posited that organic solvent would a better medium than deionized water for solvothermal treatment due to its higher viscosity and boiling point [24]. In addition, organic lithium salt is a better match with organic than inorganic media; all these factors explain why the SEM photos for C_6H_5COOLi and $C_5H_7LiO_2$ display superior specimens.

TEM characterization was employed to judge the role of organic lithium salt; the photos are displayed in Fig. 4 and further confirm the primary particle morphology of the samples. Nano-sized particles are visible for the C_6H_5COOLi sample (Fig. 4a). A distinct carbon layer can even be observed on partial particles (Fig. 4b). Plate-like particles were visible for samples with CH_3COOLi and C_5H_7OOLi, consistent with SEM data, and no obvious carbon layer was visible (Fig. 4c,d). Hence, decomposition of benzoyloxy provides in situ carbon coating during solvothermal treatment. Scheme 1 illustrates this mechanism of formation. Due to the good polarity matching of benzoyloxy in EG solvent, benzoyloxy adheres to the originally formed $LiMnPO_4$ particles. Then, under high temperature and pressure, the amorphous carbon from decomposed benzoyloxy contributes to the development of this favorable configuration.

3.2. Electrochemical behavior of $LiMnPO_4$

In previous studies, $LiMnPO_4$, showed almost no electrochemical behavior without doping or carbon coating. To improve the conductivity and crystallization of samples obtained using a solvothermal process, we selected sucrose as a carbon source. $LiMnPO_4$ and sucrose were milled for 1 h before heat-treatment. Fig. 5 displays the resulting SEM photos: a)–c) and d)–f) were C_6H_5COOLi and $C_5H_7LiO_2$, respectively, as the lithium salt, with a sucrose weight ratio of 9:1, 8:2, 7:3. Notably, the samples with 20% and 30% sucrose still showed nano-sized morphologies. Sucrose successfully prevented particle growth during subsequent calcination. However, when 40% sucrose was added, obvious large particles were visible, indicating that too much of the carbon source destroys the pre-morphology of samples and can even lead to agglomeration. The carbon content determined by the carbon–sulfur analyzer was shown in Table 1, the carbon content for as-prepared $LiMnPO_4$ with C_6H_5COOLi and $C_5H_7LiO_2$ was about 1.78%, 0.29%. This further revealed the existence of in situ carbon developed in the solvothermal process. After subsequent calcination with sucrose, the carbon content raised with the increasing amount of sucrose used.

To analyze the lithium diffusion constant, EIS measurements were performed. All Nyquist plots shown in Fig. 6a) and c) are composed of a semicircle and a line in the low-frequency region. The semicircle is related to the charge transfer between the electrolyte and the active material. The straight line at the low frequency is attributed to the diffusion of lithium ions. The lithium diffusion coefficient $\tilde{D}$ in the electrode can be calculated using Equation (1) [25,26].

$$\tilde{D} = \frac{R^2T^2}{2A^2n^4F^4C^2\sigma^2} \quad (1)$$

where T is the room absolute temperature, R is the gas constant, A is the surface area of the electrode, F is the Faraday constant, n is the number of electrons per molecule attending the electronic

Table 1
Carbon content for $LiMnPO_4$ samples before and after heat-treatment with varying sucrose concentrations.

	Solvothermal	20% sucrose	30% sucrose	40% sucrose
C_6H_5COOLi	1.78	3.59	4.93	6.49
$C_5H_7LiO_2$	0.29	2.24	3.51	4.78

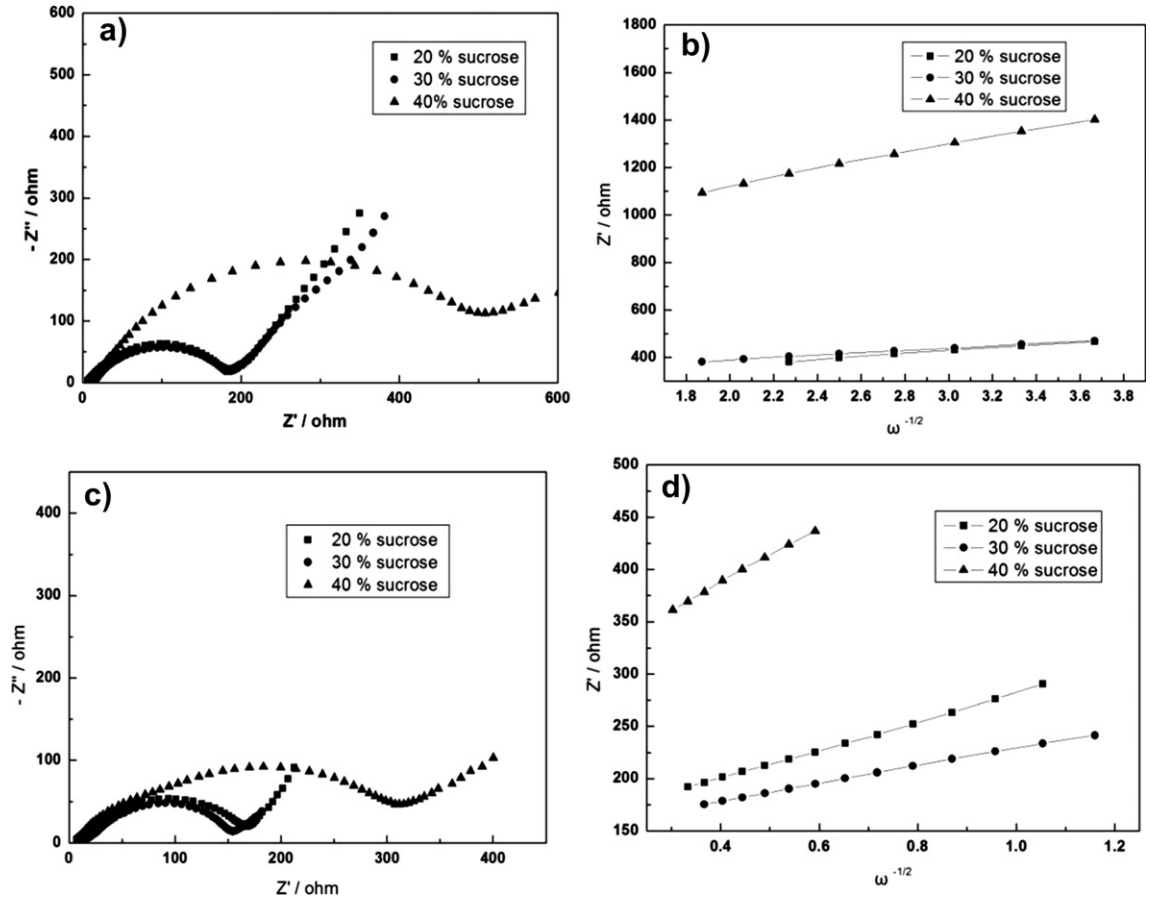

Fig. 6. Electrochemical impedance spectral characterization of samples in an open circuit and graph of Z' plotted against ω^{-1}: a, b) C_6H_5COOLi: c), d) $C_5H_7LiO_2$.

Table 2
Lithium diffusion constant ($cm^2\ s^{-1}$) for $LiMnPO_4$ samples with varying sucrose concentrations.

	20% sucrose	30% sucrose	40% sucrose
C_6H_5COOLi	2.71×10^{-13}	4.15×10^{-13}	3.40×10^{-14}
$C_5H_7LiO_2$	5.44×10^{-14}	1.40×10^{-13}	1.45×10^{-14}

transfer reaction, and C is the concentration of lithium ion in the $LiMnPO_4$ electrode. The plots of Z_{re} against $\omega^{-1/2}$ are in Fig. 6 b) and d), according to Equation (2), and σ is the slope of the straight line.

$$Z'' = \sigma\omega^{-1/2} \tag{2}$$

It is clear that the Rct for samples with 40% sucrose is much larger than the other two samples due to the agglomerated particles. The lithium diffusion coefficients $\tilde{D}$ ($cm^2\ S^{-1}$) are shown in Table 2; the two samples with 30% sucrose clearly give the best results, and we therefore conducted the subsequent charge–discharge characterization on these two samples.

The charge–discharge plots of the $LiMnPO_4$/C composite as the cathode material of lithium ion battery are provided in Fig. 7a). The test was conducted at 0.1 C over a voltage range of 2.5–4.5 V. It was

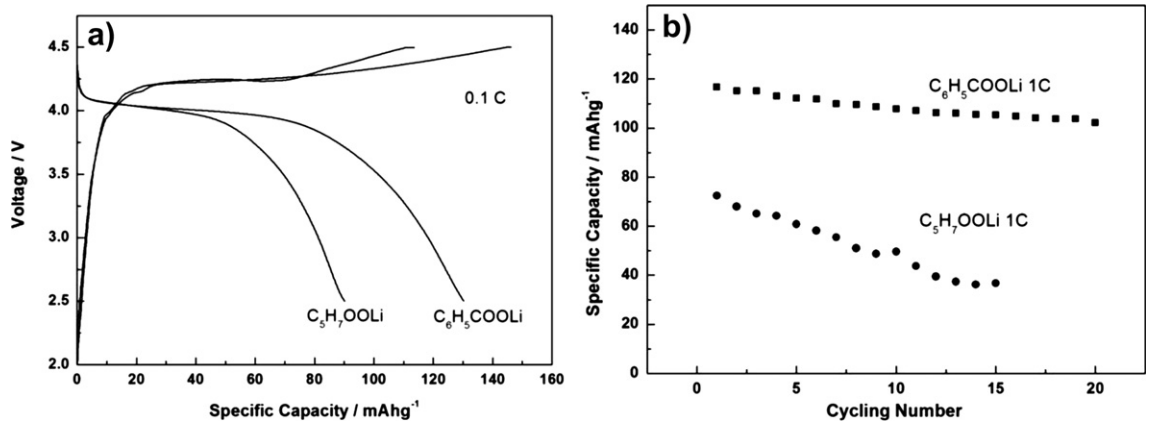

Fig. 7. a) Charge–discharge curves at 0.1 C; b) cycling ability at 1 C.

obvious that all samples showed a flat voltage at approximately 4.1 V, indicating a two-phase exchange between $LiMnPO_4$ and $MnPO_4$. Previous literature examples exhibited a sloping curve that may be caused by low electronic conductivity [27]. The initial discharge capacity for C_6H_5COOLi and C_5H_7OOLi was 130 mAh g^{-1} and 95 mAh g^{-1}, respectively.

Fig. 7b) shows the cycling ability at 1 C over a voltage range of 2.5–4.5 V. The initial capacity for C_6H_5COOLi was 115 mAh g^{-1}, and 88% of this capacity was retained after 20 cycles. Clearly, the electrochemical performance of C_5H_7OOLi was inferior to C_6H_5COOLi. Hence, in situ decomposed carbon connects particles in an electronic conductivity net. However, the Jahn–Teller-active Mn^{3+} ion of $LiMnPO_4$ and intrinsic low ionic conductivity had an adverse effect on cycling stability. Hence, there are several previous studies on hydrothermal/solvothermal method preparing $LiMnPO_4$ with cation doping, and the results revealed the improvement in cycling and rate capability. L. J. Gao et al. illustrated the effect of copper doping on $LiMnPO_4$ prepared via hydrothermal method. It suggested 2% Cu doped $LiMnPO_4$ displayed highest discharge capacity of 121 mAh g^{-1} at 0.1 C and highest capacity retention of 94% after 20 cycles [9]. Our future research will focus on improving the electrochemical performance of cation doping $LiMnPO_4$ via this solvothermal method.

4. Conclusion

Nano-sized $LiMnPO_4$ particles can be prepared via a hydrothermal method with organic lithium salt as the starting material. SEM and TEM revealed that this lithium salt is the best match with organic solvent to control particle size. Moreover, the decomposition of C_6H_5COOLi develops an in situ carbon layer on particles during the hydrothermal process. Through subsequent heat-treatment, $LiMnPO_4$/C with C_6H_5COOLi showed a discharge capacity of 130 mAh g^{-1}. The cycling ability for this material can likely be improved through further research.

References

[1] J.K. Kim, C.R. Shin, J.R. Ahn, A. Matic, P. Jacobsson, Electrochem. Commun. 13 (2011) 1105–1108.
[2] N.H. Kwon, T. Drezen, I. Exnar, I. Teerlinck, M. Isono, M. Graetzel, Electrochem. Solid-State Lett. 9 (6) (2006) A277–A280.
[3] S.K. Martha, B. Markovsky, J. Grinblat, Y. Gofer, O. Haik, E. Zinigrad, D. Aurbach, T. Drezen, D. Wang, G. Deghenghi, I. Exnar, J. Electrochem. Soc. 156 (7) (2009) A541–A552.
[4] A.K. Padhi, K.S. Nanjundaswamy, J.B. Goodenough, J. Electrochem. Soc. 144 (1997) 1188–1194.
[5] T. Drezen, N.H. Kwon, P. Bowen, I. Teerlinck, M. Isono, I. Exnar, J. Power Sources 174 (2007) 949–953.
[6] C.A.J. Fisher, V.M.H. Prieto, M.S. Islam, Chem. Mater. 20 (2008) 5907–5915.
[7] H.H. Chang, C.C. Chang, H.C. Wu, Z.Z. Guo, M.H. Yang, Y.P. Chiang, H.S. Sheu, N.L. Wu, J. Power Sources 158 (2006) 550–556.
[8] M. Higuchi, K. Katayama, Y. Azuma, M. Yukawa, M. Suhara, J. Power Sources 119 (2003) 258–261.
[9] J.F. Ni, L.J. Gao, J. Power Sources 196 (2011) 6498–6501.
[10] A. Eftekhari, J. Electrochem. Soc. 151 (2004) A1816–A1819.
[11] A. Yamada, S.C. Chung, J. Electrochem. Soc. 148 (8) (2001) A960–A967.
[12] A.M. Hashambhoya, J.F. Whitacrea, J. Electrochem. Soc. 158 (2011) A390–A395.
[13] C. Delacourt, L. Laffont, R. Bouchet, C. Wurn, J.B. Leriche, M. Morcrette, J.M. Tarascon, C. Masquelier, J. Electrochem. Soc. 152 (2005) A913–A921.
[14] S.Y. Chung, J.T. Bloking, Nat. Mater. 2 (2002) 123–128.
[15] G. Li, H. Azuma, M. Tohoda, Electrochem. Solid-State Lett. 5 (2002) A135.
[16] J. Molenda, W. Qjczyk, J. Marzec, J. Power Sources 174 (2007) 689–694.
[17] Y.K. Sun, S.M. Oh, H.K. Park, B. Scrosati, Adv. Mater. 23 (2011) 5050–5054.
[18] H.S. Fang, L.P. Li, Y. Yang, G.F. Yan, G.S. Li, Chem. Commun. (2008) 1118–1120.
[19] T. Li, T. Mei, Y.C. Zhu, H.X. Gong, T. Huang, Y.T. Qian, Chem. Lett. 40 (2011) 837–839.
[20] D. Rangappa, K. Sone, Y. Zhou, J. Mater. Chem. 21 (2011) 15813–15818.
[21] Y.G. wang, Y.R. wang, E. Hosono, K.X. Wang, H.S. Zhou, Angew. Chem. 120 (2008) 7571–7575.
[22] G.C. Liang, L. Wang, X. Qu, X. Zhao, S.Z. Xu, J. Power Sources 184 (2008) 538–542.
[23] A.V. Murugan, T. Muraliganth, A. Manthiram, J. Electrochem. Soc. 156 (2) (2009) A79–A83.
[24] H.S. Fang, L.P. Li, G.S. Li, Chem. Lett. 36 (2007) 436–437.
[25] K. Saravanan, V. Ramar, P. Balaya, J.J. Vittal, J. Mater. Chem. 11 (2011) 14925–14935.
[26] X.Z. Liao, Z.F. Ma, Q. Gong, Y.S. He, L. Pei, L.J. Zeng, Electrochem. Commun. 10 (2008) 691–694.
[27] Jiali Liu, Dongge Hu, Tao Huang, Aishui Yu, J. Alloys Compd. 518 (2012) 58–62.